S1: Lattice parameters and illustrations of the bulk crystal structures:

Form.	Structure	a(calc/exp)	b(calc/exp)	c(calc/exp)	angle(calc/exp)
TiO_2	Rutile (tetragonal)	4.682 4.594[e[1]]	-	2.974 2.959	-
SiO_2	α quartz (hexagonal)	4.991 4.916[t[2]]	-	5.500 5.405	-
SnO_2	Rutile (tetragonal)	4.864 4.737[e[1]]	-	3.249 3.186	-
NbO_2	Rutile (tetragonal)	4.980 4.85[e[3]]		2.943 3.03	
γ-Al_2O_3	Monoclinic	5.637 5.587[t[4]]	8.613 8.413	8.068 8.068	90.012 90.590
δ-Ta_2O_5	Hexagonal	7.366 7.248[e[5]]	-	3.907 3.880	-
α-Nb_2O_5	Monoclinic	21.56 21.16[e[6]]	3.847 3.822	19.58 19.35	119.61 119.50
ZrO_2	Monoclinic	5.211 5.150[e[7]]	5.278 5.212	5.387 5.315	99.38 99.23

Table 1: The calculated and experimental (e) lattice parameters. Where no experimental information was available, other theoretical (t) values have been used for comparison.

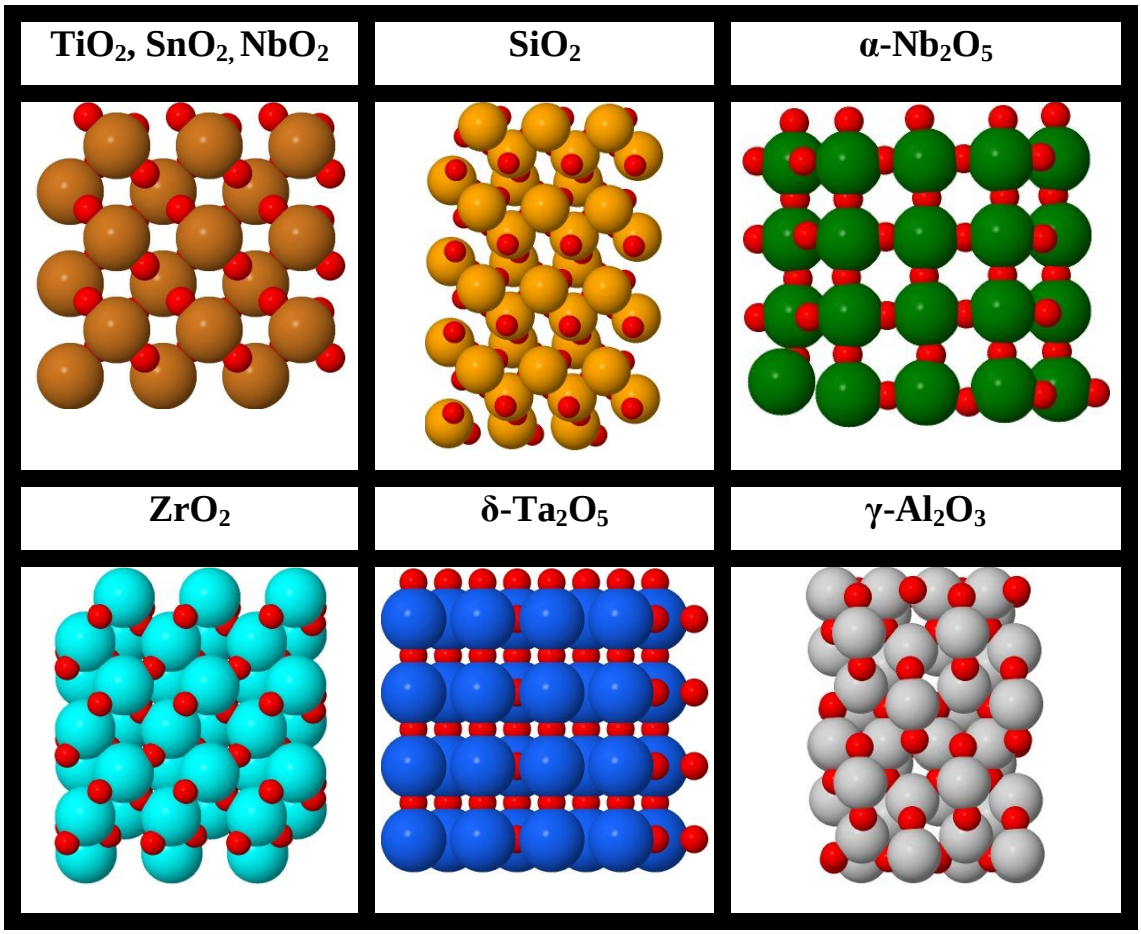

Figure 1: Illustrations of the most stable bulk crystal structures of the metal oxides.

S2: Stability plots

Stability diagrams for the most close-packed surface terminations, different rutile steps and for the PtO_x adsorption on the steps and in the first surface layer are shown in the figures below. The figures were made by adding (or subtracting) oxygen atoms to (or from) the metal oxide surfaces with the stoichiometric ratio of metal and oxygen atoms.
The adsorption values at U = 0 V were calculated with use of Eq. (1).

$$\Delta G_{U=0}\left(xO^{*}\right) = G(MO + xO^{*}) - G(MO) - xG(H_2O) + xG(H_2), \qquad (1)$$

in which x represents the number of adsorbed oxygen atoms. The free energy dependence on potential is obtained by relating the free energy of protons and electrons to the free energy of hydrogen in the gas phase according to the Standard Hydrogen Electrode (SHE) concept. [8] Following this concept the free energy value of $\Delta G_U\left(xO^{*}\right)$ at any potential is given by Eq. (2).

$$\Delta G_U\left(xO^{*}\right) = \Delta G_{U=0}\left(xO^{*}\right) - 2xU \qquad (2)$$

Similar equation was used to calculate the free energies of oxygen vacancies at varying U.

$$\Delta G_U\left(xO_{vac}\right) = \Delta G_{U=0}\left(xO_{vac}\right) + 2xU \qquad (3)$$

Stability plots for the most stable metal oxide surface terminations

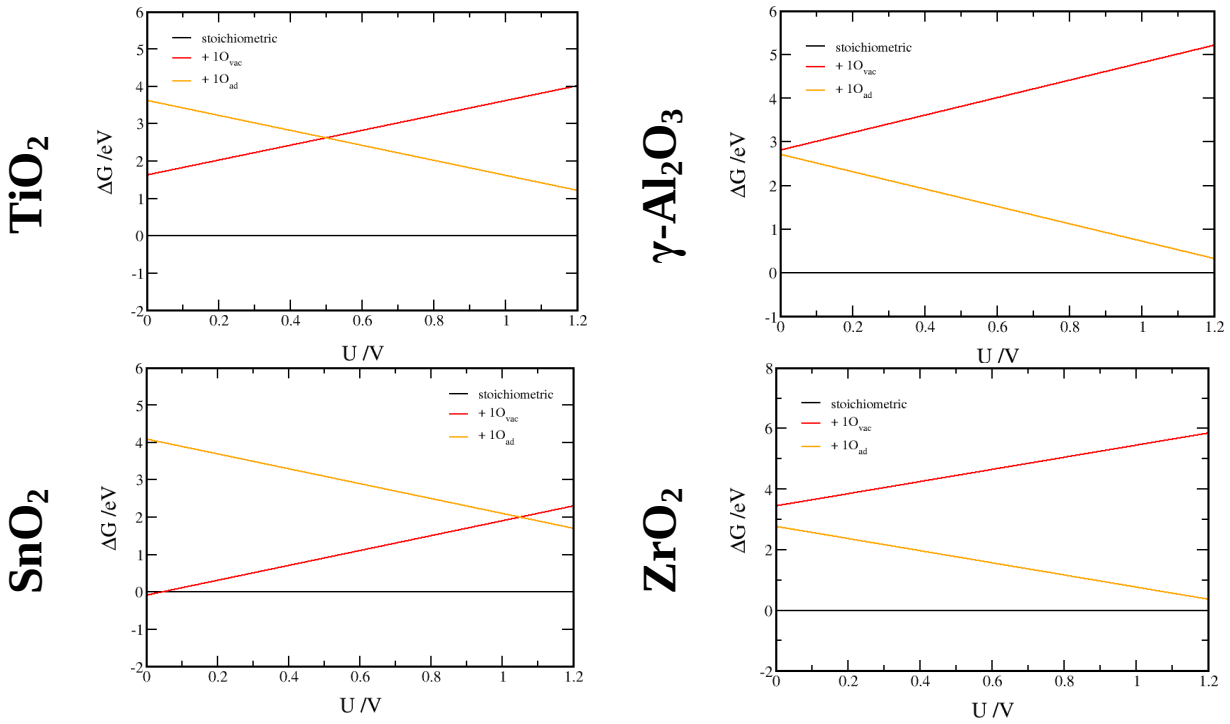

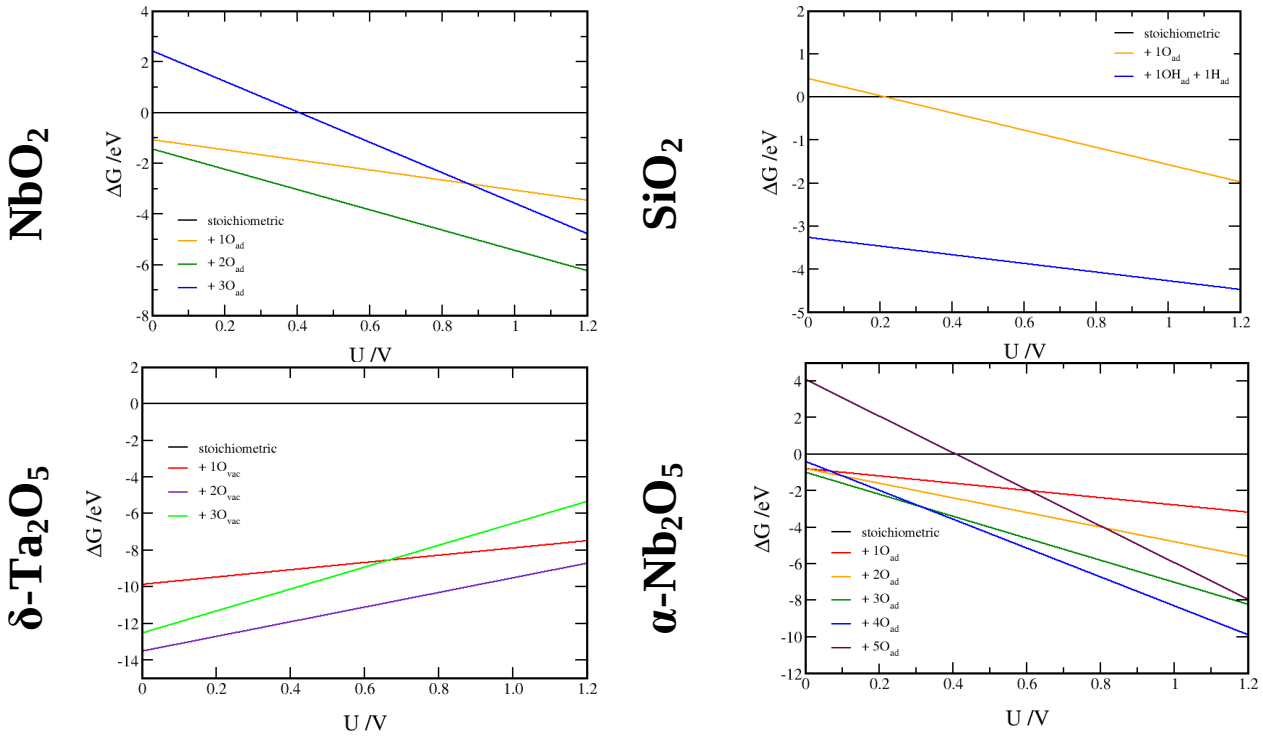

Figure 2: Stability plots for the most stable metal oxide surfaces. The equilibrium surfaces at U = 0.85 – 0.96 V correspond to the lowest free energy lines in this range.

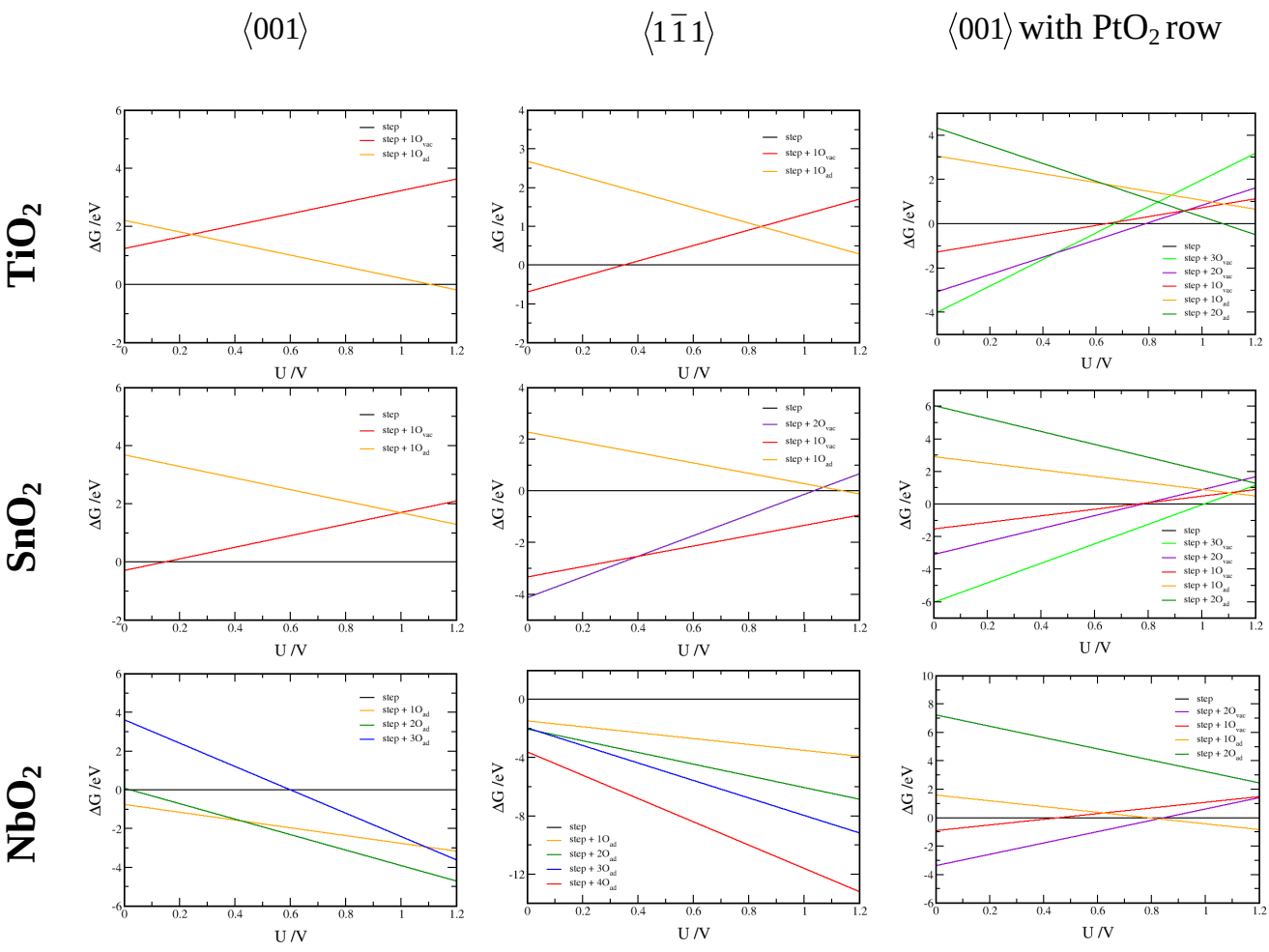

Figure 3: Stability plots for the rutile step surfaces, $\langle 001 \rangle$ and $\langle 1\bar{1}1 \rangle$ with and without an additional PtO_2 row.

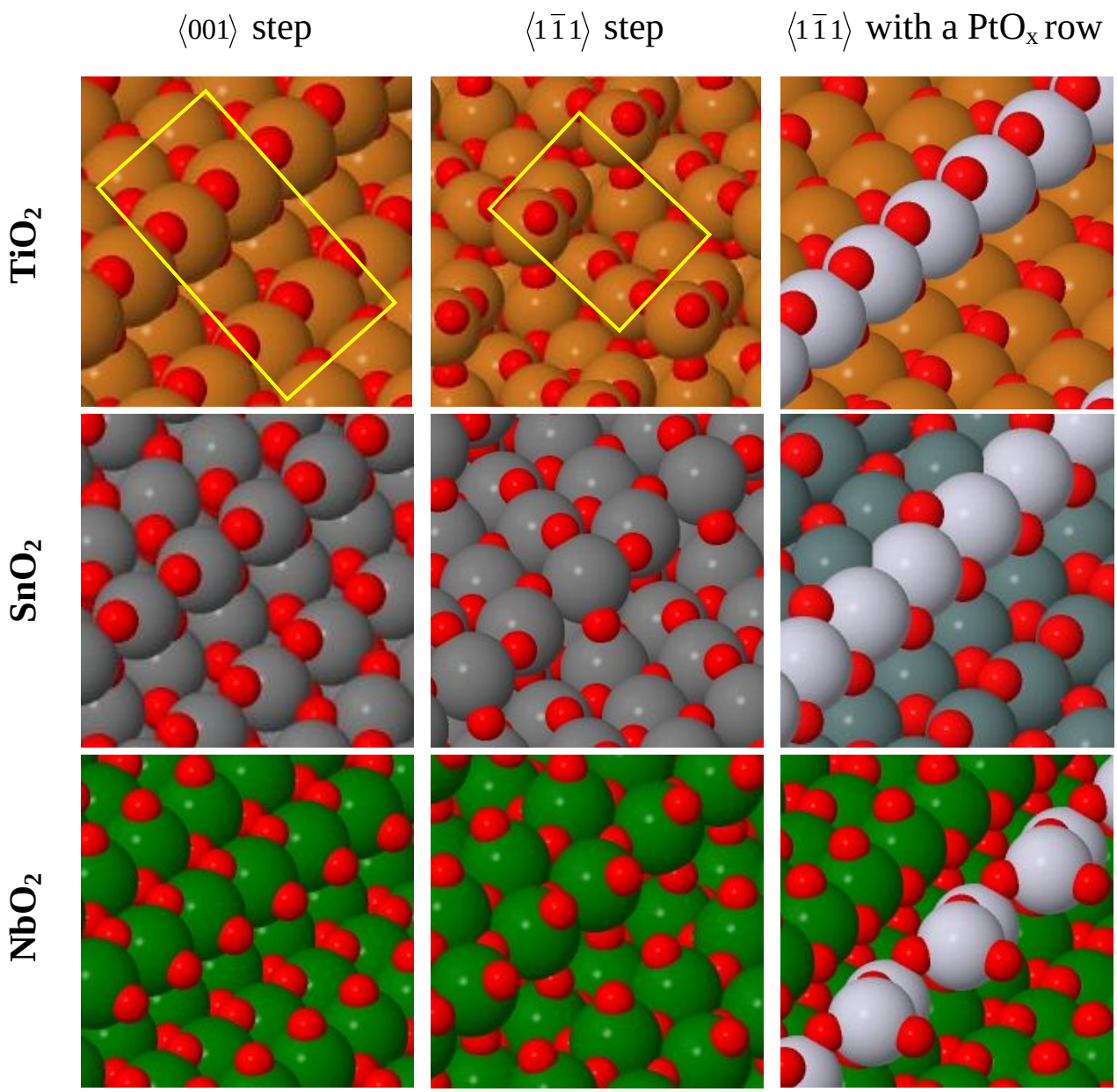

Figure 4: The most stable rutile step surfaces at U = 0.85 - 0.96 V. The first two columns show the snapshots of $\langle 001 \rangle$ *and* $\langle 1\bar{1}1 \rangle$ *steps, while the third column shows the illustrations of the* $\langle 001 \rangle$ *surfaces with an additional* PtO_x *row. The boxes denote the unit cells sizes with the smallest periodicity.*

Stability plots for the most stable metal oxide surfaces in which one unit oxide unit is substituted with Pt_jO_k.

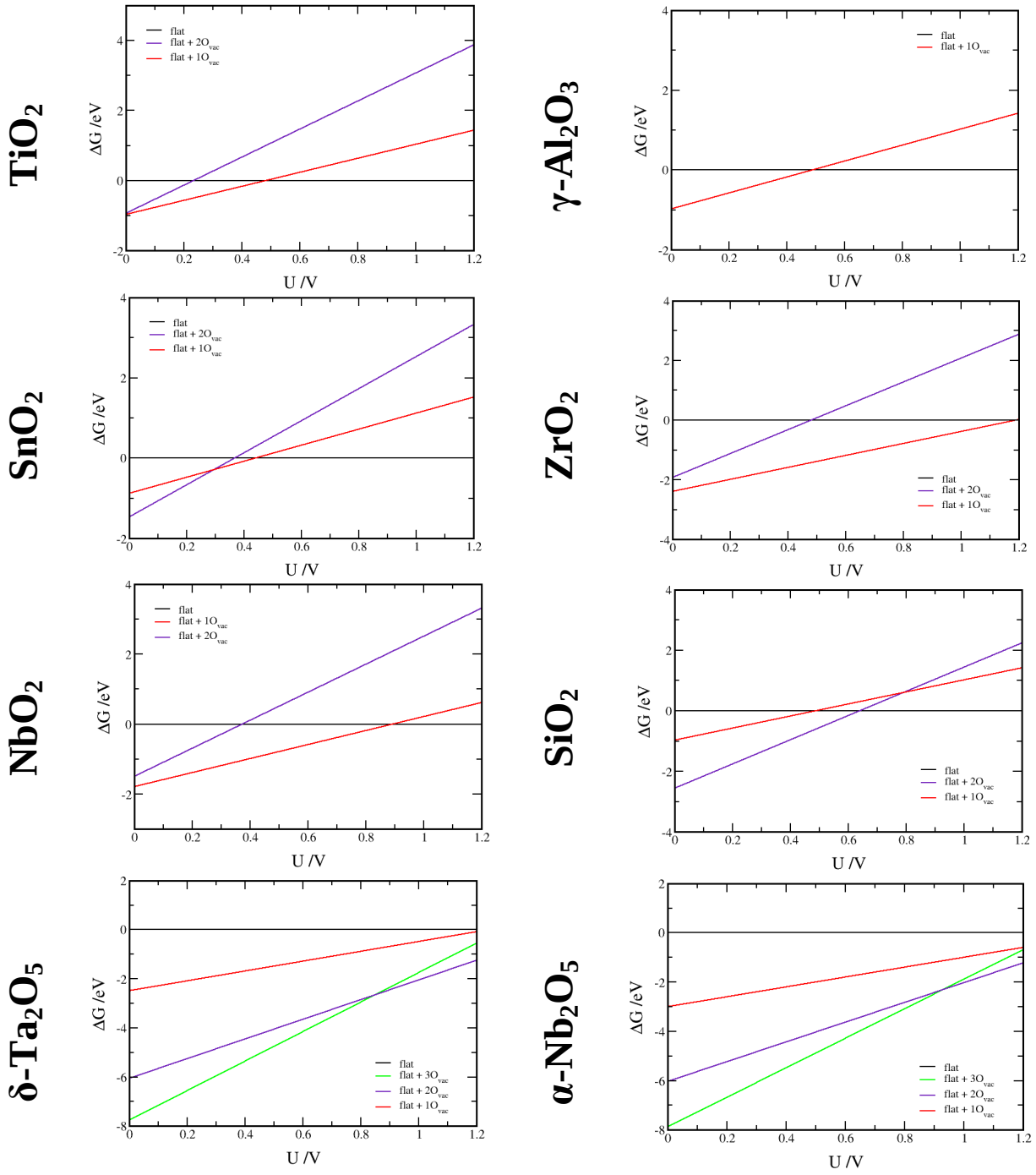

Figure 5: Stability plots for PtO_2 adsorbed in the first layer of the metal oxide 110 surfaces.

1 C. J. Howard; T. M. Sabine; F. Dickson, *Acta. Cryst.* **47** (1991) 462.

2 N. R. Keskar, J. R. Chelikowsky, *Condensed Matter* **46** (1992) 1.

3 A. A. Bolzan, C. Fong, B. J. Kennedy, C. J. Howard, *Acta Crystallogr., Sect. B: Struct. Sci.* **B53** (1997) 373.

4 X. Krokidis, P. Raybaud, A.-E. Gobichon, B. Rebours, P. Euzen, H. Toulhoat, *J. Phys. Chem. B* **105** (2001) 5121.

5 N. Terao, *Jpn. J. Appl. Phys.* **6** (1967) 21.

6 B. M. Gatehouse, A. D. Wadsley, *Acta Cryst.* **17** (1964) 1545.

7 C. J. Howard, E. H. Kisi, R. B. Roberts, R. J. Hill, *J. Am. Ceram. Soc.* **73** (1990) 2828.

8 J. K. Nørskov, J. Rossmeisl, A. Logadottir, L. Lindqvist, J. R. Kitchin, T. Bligaard, H. Jónsson, *J. Phys. Chem. B* **108** (2004) 17886.